

Cl_nH_{6-n}SiGe Compounds for CMOS Compatible Semiconductor Applications: Synthesis and Fundamental Studies

Jesse B. Tice, Andrew V. G. Chizmeshya, Radek Roucka, John Tolle, Brian R. Cherry, and John Kouvetakis*

Contribution from the Department of Chemistry/Biochemistry, Arizona State University, Tempe, Arizona 85287-1604

Received February 26, 2007; E-mail: jkouvetakis@asu.edu

Abstract: We describe the synthesis of a new family of chlorinated Si–Ge hydrides based on the formula Cl_nH_{6-n}SiGe. Selectively controlled chlorination of H₃SiGeH₃ is provided by reactions with BCl₃ to produce ClH₂SiGeH₃ (**1**) and Cl₂HSiGeH₃ (**2**). This represents a viable single-step route to the target compounds in commercial yields for semiconductor applications. The built-in Cl functionalities are specifically designed to facilitate selective growth compatible with CMOS processing. Higher order polychlorinated derivatives such as Cl₂SiHGeH₂Cl (**3**), Cl₂SiHGeHCl₂ (**4**), ClSiH₂GeH₂Cl (**5**), and ClSiH₂GeHCl₂ (**6**) have also been produced for the first time leading to a new class of highly reactive Si–Ge compounds that are of fundamental and practical interest. Compounds **1–6** are characterized by physical and spectroscopic methods including NMR, FTIR, and mass spectroscopy. The results combined with first principles density functional theory are used to elucidate the structural, thermochemical, and vibrational trends throughout the general sequence of Cl_nH_{6-n}SiGe and provide insight into the dependence of the reaction kinetics on Cl content in the products. The formation of **1** was also demonstrated by an alternative route based on the reaction of (SO₃CF₃)SiH₂GeH₃ and CsCl. Depositions of **1** and **2** at very low temperatures (380–450 °C) produce near stoichiometric SiGe films on Si exhibiting monocrystalline microstructures, smooth and continuous surface morphologies, reduced defect densities, and unusual strain properties.

Introduction

The chlorination of Si–Ge hydrides to form volatile and highly reactive Cl-substituted analogues represents an unexplored area of precursor synthesis with tremendous potential in modern semiconductor device development. The benefits of this strategy are already evident by the widespread commercial use of chlorosilanes in selective growth of high performance Si-based electronic materials. In the topical SiGe alloy arena,¹ new materials with Ge-rich compositions are being vigorously developed to enable higher speed in microprocessors,² lower power consumption in cell phones,³ silicon-based photonics,⁴ and more efficient solar cells.⁵ However, for selective growth applications the currently available synthetic strategy, involving multisource reactions of chlorosilanes and germanes, might not provide compositional control and requires high-temperature growth which is incompatible with CMOS-based processing of small features on patterned wafers. In view of the increasing demand for very low-temperature selective growth of Si_{1-x}Ge_x for high frequency applications, new approaches to circumvent the above challenges are highly desirable.

We have recently developed a CVD method that allows for the first time the growth of Ge-rich (Ge ≥ 50 atom %) device-quality alloys on Si that cannot be obtained by conventional routes.^{6–8} Our breakthrough technology utilizes previously unknown designer Si–Ge hydrides such as the silyl–germyl sequence of molecules [(H₃Ge)_xSiH_{4-x}, x = 1–4], which are obtained in viable high-purity yields via straightforward synthetic methodologies developed in our labs.⁶ The inherent incorporation of the entire SiGe, SiGe₂, SiGe₃, and SiGe₄ molecular cores of the H₃GeSiH₃, (H₃Ge)₂SiH₂, (H₃Ge)₃SiH, and (H₃Ge)₄Si compounds into the films provides unprecedented control of morphology, composition, and strain. Our ongoing work in this area addresses a critical need for precursors and processes that yield high quality semiconductors under conditions compatible with modern device fabrication and processing.

The successful application of the (H₃Ge)_xSiH_{4-x} family of compounds suggests that the synthesis of Cl_nH_{6-n}SiGe analogues (via controlled chlorination of their simplest constituent member SiH₃GeH₃) should produce compounds such as ClSiH₂GeH₃ (**1**) and Cl₂SiHGeH₃ (**2**) (Figure 1) which are designed to provide significant benefits from a selective area growth

(1) Mooney, P. M.; Chu, J. O. *Annu. Rev. Mater. Sci.* **2000**, *30*, 335.
(2) Luryi, S.; Xu, J.; Zaslavsky, A. *Future Trends in Microelectronics: Up the Nanocreek*; Wiley: New York, 2007.
(3) Heftman, G.; Grossman, S.; Day, J. *Power Electron. Technol.* **2003**, 44–46.
(4) Jalali, J.; Paniccia, M.; Reed, G. Silicon Photonics. *IEEE Microwave Magazine* **2006**, *7*, 1440.
(5) Green, M. A. Third generation photovoltaics: Ultra-high conversion efficiency at low cost. *Prog. Photovoltaics* **2001**, *9*, 123.

(6) Ritter, C. J.; Hu, C.; Chizmeshya, A. V. G.; Tolle, J.; Klewer, D.; Tsong, I. S. T.; Kouvetakis, J. *J. Am. Chem. Soc.* **2005**, *127* (27), 9855.
(7) Hu, C.-W.; Menendez, J.; Tsong, I. S. T.; Tolle, J.; Chizmeshya, A. V. G.; Ritter, C.; Kouvetakis, J. *Appl. Phys. Lett.* **2005**, *87* (18), 181903.
(8) Chizmeshya, A. V. G.; Ritter, C. J.; Hu, C.-W.; Tolle, J.; Nieman, R.; Tsong, I. S. T.; Kouvetakis, J. *J. Am. Chem. Soc.* **2006**, *128* (21), 6919.

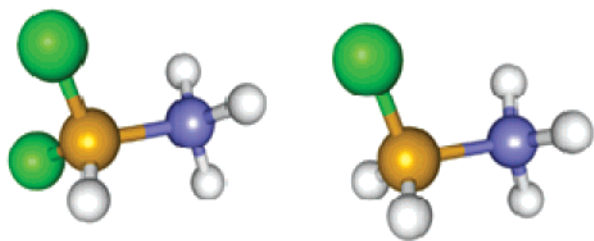


Figure 1. Structural representations of ClH₂SiGeH₃ and Cl₂HSiGeH₃ molecules. Si, Ge, Cl, and H are depicted as gold, blue, green, and white spheres, respectively.

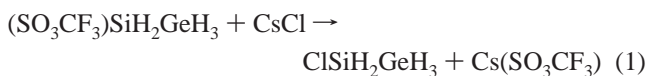
perspective compared to current approaches based on high-temperature reactions of chlorinated silanes. In general, it has been suggested that selective growth of Si or Si–Ge films can be achieved by in situ use of chlorinating etchants derived from these reactions. These etchants remove the amorphous material typically deposited on masked features (in a blanket deposition step) at a much higher rate than they remove crystalline material grown on the oxide-free regions. Thus, they promote selective growth on the unmasked areas around the patterned regions on the wafer. The newly introduced ClSiH₂GeH₃ and Cl₂SiHGeH₃ compounds could also function as built-in cleaning agents for the removal of amorphous material at relatively low temperatures during in situ selective growth of a variety of device structures on patterned Si wafers.

CVD reactions of halogenated Si compounds are described by numerous patent applications to be problematic due to contamination of the deposited material by residual Cl impurities and undesirable particulates. In the new single sources, **1** and **2**, the built-in composition and the high reactivity provide precise control with regard to complete HCl elimination and simultaneously enable incorporation of the desired SiGe content in the purest possible form. Finally, the larger mass of the halogenated silylgermanes provides an increased kinetic stability allowing growth to be conducted at even lower temperatures than the corresponding SiH₃GeH₃ hydride.

This report describes the preparation and properties of the new compounds ClSiH₂GeH₃ (**1**) and Cl₂SiHGeH₃ (**2**). Their use to deposit stoichiometric SiGe films on Si at very low temperatures (370–450 °C) is also described. En route to **1** and **2** we have produced an entire new series of multiply chlorinated derivatives with intriguing bonding properties and potential applications in low-temperature synthesis of Si–Ge optoelectronic alloys.

Results and Discussion

(a) Synthetic Routes to ClH₂SiGeH₃ (1**) and Cl₂SiHGeH₃ (**2**).** The synthesis of ClH₂SiGeH₃ (**1**) was initially conducted by reaction of CsCl with the triflate substituted silylgermane (SO₃CF₃)SiH₂GeH₃ (eq 1).



Decane was used as the solvent, and the overall yield was ~60%. The (SO₃CF₃)SiH₂GeH₃ starting material was prepared by direct reaction of PhSiH₂GeH₃ and HSO₃CF₃ in the absence of solvent at –35 °C. Pure ClH₂SiGeH₃ (**1**) was conveniently isolated by vacuum distillation from the solid Cs(SO₃CF₃) byproduct, as a colorless, pyrophoric liquid with a room-

temperature vapor pressure of ~150 Torr. Due to its high reactivity, compound **1** was characterized by physical methods such as mass spectrometry, FTIR, and NMR, rather than conventional elemental analyses. The mass spectra were obtained by direct insertion and revealed an isotopic envelope centered at 141 amu corresponding to the molecular ion, and a fragmentation pattern consistent with the proposed molecular structure ClSiH₂GeH₃. The IR spectra obtained from measurements on gaseous samples showed the expected Si–H and Ge–H stretching bands split into a set of doublets at 2183, 2169 and 2082, 2070 cm^{–1}, respectively. The bending modes between 950 and 540 cm^{–1} are also split into doublets. A complete first principles analysis of the vibrational properties indicated that the observed IR spectra compare well with the simulated analogues as described in detail in a later section. The NMR spectra showed the GeH₃ proton resonance as a triplet at 3.12 ppm, the SiH₂ proton resonance as a quartet at 4.68 ppm, and the ²⁹Si resonance as a singlet at –24.61 ppm. The proton peaks are shifted downfield with respect to the corresponding GeH₃ (3.06 ppm) and SiH₃ (3.40 ppm) signatures of SiH₃GeH₃, consistent with the substitution of H on the Si atom by the electron withdrawing Cl atom. Moreover a proton-decoupled ¹H–²⁹Si HMQC (heteronuclear multiple quantum coherence) spectrum showed that the H atoms at 4.68 ppm are directly attached to Si atom at –24.61 ppm which confirms the molecular structure. These interpretations are corroborated with our prior NMR studies of the related SiH_{4–x}(GeH₃)_x family of compounds.⁶

NMR samples kept for several days showed no additional signals due to impurities or decomposition byproducts, indicating that the solutions of the compound remain stable and pure. Multigram batches of liquid **1** kept at 22 °C also showed no discernible decomposition over extended time periods, to form HCl, chlorosilanes, or germanium hydride polymers, indicating that the compound is remarkably robust in its pure physical form. We note that an alternative synthesis of **1** was also performed using PhSiH₂GeH₃ and HCl (eq 2).



However, due to the similarity in boiling points, **1** could not be separated by fractional distillation from the benzene byproduct. Furthermore, the overall yield of **1** was found to be too low for applications in materials synthesis, and this route therefore was not pursued any further.

A complicating factor in the synthetic route describe by eq 1 is that overall yields of pure (SO₃CF₃)SiH₂GeH₃ are severely limited. This can be traced to the low yields (maximum 25%) obtained in forming PhSiH₂GeH₃ from the reaction of PhSiH₂Cl and KGeH₃. Furthermore, (SO₃CF₃)SiH₂GeH₃ is highly reactive and therefore difficult to handle, making its purification and storage for subsequent use challenging. In fact, the compound has inexplicably and randomly exploded during synthesis while following the same routine preparation and isolation procedures.

There are numerous examples of silane and germane halogenation reactions reported to date using a variety of methods.^{9–15}

- (9) Drake, J. E.; Goddard, N. *Inorg. Nucl. Chem. Lett.* **1968**, *4*, 385.
 (10) Mackay, K. M.; Robinson, P.; Spanier, E. J.; MacDiarmid, A. G. *J. Inorg. Nucl. Chem.* **1966**, *28*, 1377.
 (11) Swiniarski, M. F.; Onyszczuk, M. *Inorg. Synth.* **1974**, *15*, 157. (b) Becker, G.; Holderich, W. *Chem. Ber.* **1975**, *108*, 2484.

Our search for a viable, straightforward, and safe synthetic methodology that is also scalable from an industrial perspective to produce Si–Ge analogues has led to the development of a single-step route utilizing the commercially available starting materials BCl_3 and SiH_3GeH_3 . When BCl_3 and SiH_3GeH_3 are combined in a 1:3 molar proportion, we find that all of the BCl_3 reactant is consumed and a stoichiometric amount of B_2H_6 is produced according to eq 3.

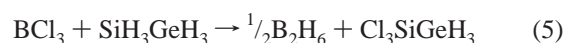


The target $\text{ClSiH}_2\text{GeH}_3$ (**1**) compound was obtained by trap-trap fractionation in significant yields (~60–70%) and was identified by spectroscopic methods as described above. However, in addition to **1**, the disubstituted derivative $\text{Cl}_2\text{-HSiGeH}_3$ (**2**) was isolated and purified in small amounts as a byproduct in the reaction mixture. The NMR spectra of the mixture prior to separation showed that a ratio of 12:1 of monochloro to dichloro is typically produced. The GeH_3 NMR resonance of **2** was observed as a doublet at 3.25 ppm and the SiH resonance as a quartet at 5.57 ppm which is consistent with a second substitution of Cl on the Si site. The ^1H – ^{29}Si HMQC spectrum also determined that the proton (5.57 ppm) is bound to the Si atom (+9.77 ppm). The integrated SiH/ GeH_3 peak intensity ratio is 1:3, as expected. Compound **2** was further characterized by gas-phase IR and mass spectrometry. These spectroscopic results combined with DFT theoretical simulations of the IR spectra (described below) confirm the proposed $\text{Cl}_2\text{SiHGeH}_3$ molecular structure.

(b) Higher Order Chlorination of H_3SiGeH_3 . The presence of $\text{Cl}_2\text{SiHGeH}_3$ (**2**) as a minor component in the above reaction prompted us to explore stoichiometric reactions of BCl_3 and SiH_3GeH_3 in a 2:3 molar ratio to promote its formation as the primary product (see eq 4).



This reaction was carried out at 0 °C for 2 h and yielded equal amounts of $\text{ClSiH}_2\text{GeH}_3$ (**1**) and $\text{Cl}_2\text{SiHGeH}_3$ (**2**) indicating that the second chlorination at the Si center is enhanced under these conditions, as expected. When the chlorine activity was further increased by combining the reactants in 1:1 molar ratio (see eq 5), the $\text{Cl}_2\text{SiHGeH}_3$ (**2**) species was predominately produced while the formation of $\text{ClSiH}_2\text{GeH}_3$ (**1**) was essentially suppressed. Under these conditions, the reaction also produced a substantial amount of a low-volatility liquid mixture which consisted primarily of the polychlorinated $\text{Cl}_2\text{SiHGeH}_2\text{Cl}$ (**3**) and $\text{Cl}_2\text{SiHGeCl}_2\text{H}$ (**4**) compounds. These were detected and characterized by NMR spectroscopy. The NMR spectra also showed trace amounts of two additional compounds which were identified to be the $\text{ClSiH}_2\text{GeH}_2\text{Cl}$ (**5**) and $\text{ClSiH}_2\text{GeHCl}_2$ (**6**) species by their ^1H and ^{29}Si resonance signatures. We note that the thermodynamically expected $\text{Cl}_3\text{SiHGeH}_3$ was not formed under these conditions, although the reaction stoichiometry was specifically tuned to promote its formation according to the reaction shown by eq 5.



The above results indicate that a distribution of multiple chlorinations occurs with increasing the amount of BCl_3 and thus the activity of Cl in the reaction. This prompted us to increase the BCl_3 concentration even further in an attempt to drive the third chlorination on the Si center. In principle, a 2:1 ratio of BCl_3 to SiH_3GeH_3 is expected to yield the limiting $\text{Cl}_3\text{-SiGeCl}_3$ perchlorinated product according to the reaction shown by eq 6.



We found however that in spite of numerous variations in reaction conditions the 2:1 stoichiometry invariably produced only higher order chlorinated derivatives in the $\text{Cl}_n\text{H}_{6-n}\text{SiGe}$ sequence rather than the hexachloro product. The main products were found to be the $\text{Cl}_2\text{HSiGeHCl}_2$ (**4**) and $\text{Cl}_2\text{SiHGeH}_2\text{Cl}$ (**3**) compounds while minor byproducts included compounds $\text{ClSiH}_2\text{GeH}_2\text{Cl}$ (**5**), $\text{ClSiH}_2\text{GeHCl}_2$ (**6**), and dichlorosilane ($\text{Cl}_2\text{-SiH}_2$). The outcome of enhancing the chlorine activity in these reactions was to substitute a maximum of two chlorines on the Si center with additional Cl atoms bonding to the Ge site of $\text{Cl}_2\text{SiHGeH}_3$. Table 1 summarizes the target and observed products obtained with increasing the Cl activity as described by eqs 3–6.

(c) Structural Trends of $\text{Cl}_n\text{H}_{6-n}\text{SiGe}$ via NMR. Among the compounds synthesized, the mono- and dichloro species **1** and **2** are readily isolated as distinct volatile liquids. However, the very close boiling points and high reactivity of the polychlorinated derivatives **3–6** precluded their individual separation by normal distillation or fractionation techniques. Accordingly, their compositions were determined and their structures were elucidated by extensive ^1H and ^{29}Si NMR analyses such as ^1H correlated spectroscopy (COSY) and ^1H – ^{29}Si HMQC techniques. The ^1H NMR spectra showed the expected multiplicity in various SiH_x and GeH_x peaks and ^{29}Si satellite peaks which exhibit $^1J_{\text{Si-H}}$ and $^2J_{\text{Si-H}}$ coupling constants with nominal values of 200–300 and 10–50 Hz, respectively. These techniques in combination with the coupling constants are particularly useful because they unambiguously establish the connectivities of the various H and Cl atoms to the Si–Ge molecular core for each compound in the various product mixtures.

Table 2 lists the ^1H and ^{29}Si chemical shifts as well as the Si–H and H–H J couplings derived from our measurements for all chlorinated compounds listed in Table 1 including the previously discussed **1** and **2** as well as the SiH_3GeH_3 reactant. We note the following trends in the chemical shift data: (a) For a fixed number of Cl atoms on the Si site, increasing the number of Cl atoms on the Ge site enhances the shielding of the SiH_x protons resulting in a systematic upfield shift of the latter. For example, in the sequence $\text{Cl}_2\text{SiHGeH}_3$, $\text{Cl}_2\text{SiHGeH}_2\text{-Cl}$, and $\text{Cl}_2\text{SiHGeHCl}_2$, the Si–H shifts are 5.57, 5.35, and 5.15 ppm, respectively (steps of ~0.2 ppm). Similarly for $\text{ClSiH}_2\text{-GeH}_3$, $\text{ClSiH}_2\text{GeH}_2\text{Cl}$, and $\text{ClSiH}_2\text{GeHCl}_2$, the SiH_2 shifts are 4.68, 4.53, and 4.38 ppm, respectively (steps of ~0.1 ppm). (b) By contrast, the GeH_x shifts are independent of the number of Cl atoms on the Si site and simply scale downfield in proportion to the number of Cl atoms on Ge site (δGeH_x : ~3.2 ppm for “– GeH_3 ”, 4.8 ppm for “– GeH_2Cl ”, and 6.0 ppm for

(12) Ward, L. G. L. *Inorg. Synth.* **1971**, *13*, 154.

(13) Ward, L. G. L.; MacDiarmid, A. G. *J. Inorg. Nucl. Chem.* **1961**, *20*, 345.

(14) Lobreyer, T.; Oeler, J.; Sundermeyer, W. *Chem. Ber.* **1991**, *124*, 2405.

(15) Van Dyke, C. H.; MacDiarmid, A. G. *J. Inorg. Nucl. Chem.* **1963**, *25*, 1503.

Table 1. Chlorination Products and Byproducts as a Function of Chlorine Activity^a

BCl ₃ :SiH ₃ GeH ₃	target product	observed products	observed byproducts
1:3	ClSiH ₂ -GeH ₃	ClSiH ₂ -GeH ₃	Cl ₂ SiH-GeH ₃
2:3	Cl ₂ SiH-GeH ₃	ClSiH ₂ -GeH ₃ , Cl ₂ SiH-GeH ₃	
1:1	Cl ₃ Si-GeH ₃	Cl ₂ SiH-GeH ₃	ClSiH ₂ -GeClH ₂ , Cl ₂ SiH-GeClH ₂ , ClSiH ₂ -GeCl ₂ H, Cl ₂ SiH-GeCl ₂ H
2:1	Cl ₃ Si-GeCl ₃	Cl ₂ SiH-GeClH ₂ , Cl ₂ SiH-GeCl ₂ H	ClSiH ₂ -GeClH ₂ , Cl ₂ SiH-GeH ₃ , ClSiH ₂ -GeCl ₂ H

^a The first column lists the ratio of BCl₃ to SiH₃GeH₃ reactants. All reactions were carried out at *T* = 0 °C for 2 h.

Table 2. ¹H and ²⁹Si Shifts and Si-H and H-H *J* Coupling Constants for Cl_nH_{6-n}SiGe Compounds^a

compd	δ ¹ H (SiH ₃)	δ ¹ H (GeH ₃)	δ ²⁹ Si	¹ J _{Si-H}	² J _{Si-H}	³ J _{H-H}
H ₃ SiGeH ₃ ^b	3.52 (q)	3.18 (q)	-91.60	204.0	7.2	3.8
ClSiH ₂ GeH ₃	4.68 (q)	3.12 (t)	-24.61	231.9		3.3
Cl ₂ SiHGeH ₃	5.57 (q)	3.25 (d)	9.77	271.9	13.1	3.0
ClSiH ₂ GeH ₂ Cl	4.53 (t)	4.86 (t)	-24.26	244.8		3.5
Cl ₂ SiHGeH ₂ Cl	5.35 (t)	4.82 (d)	3.36	290.0	29.2	4.3
ClSiH ₂ GeHCl ₂	4.38 (d)	6.12 (t)	-22.87	308.0	51.5	7.0
Cl ₂ SiHGeHCl ₂	5.15 (d)	5.97 (d)	-1.12	259.7	39.4	4.4

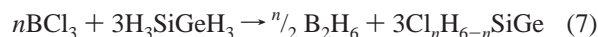
^a The assignments were made on the basis of the COSY and HMQC experiments and were confirmed by the *J*_{Si-H} (listed in Hz). ^b Reference 14.

“-GeHCl₂” roughly independent of the number of Cl attached to Si). (c) The trends in the ²⁹Si shifts are more subtle, and our study finds that for a fixed number of Cl atoms on the Si site slight downfield shifts are associated with increasing Cl atoms on the Ge site (for “ClH₂Si-” molecules, δSi are -24.6, -24.3, -22.9 for 0, 1, and 2 Cl atoms on the Ge site, respectively). (d) Furthermore, this effect becomes more pronounced as the number of Cl atoms on the Si site is increased (for “Cl₂HSi-” molecules, δSi are 9.8, 3.4, -1.1 for 0, 1, and 2 Cl atoms on the Ge site, respectively). This suggests that chlorines bonded to Ge systematically shield the Si nuclei as the number of Cl atoms is increased. (e) Some notable trends of the coupling constants are as follows: For a fixed number of chlorines on the Si site, the ¹J_{Si-H} and ³J_{H-H} values increase with increasing number of chlorines bonded to Ge. The ¹J_{Si-H} value increases with increasing the number of Si-Cl bonds in the SiH₃GeH₃, ClSiH₂GeH₃, and Cl₂SiHGeH₃ sequence, while the opposite is observed for the ³J_{H-H}. The highest ³J_{H-H} value corresponds to the most chlorinated Cl₂SiHGeHCl₂ molecule. Similar comparisons can be made for the chlorinated disilane analogues where similar trends are observed for the coupling constants ¹J_{Si-H} (197.8, 226.5, 267.7, 233.1, 277.2, 285.3) and ³J_{H-H} (3.5, 2.8, 2.1, 2.6, 2.4, 4.0) corresponding to the compounds (SiH₃-SiH₃, ClSiH₂SiH₃, Cl₂SiHSiH₃, ClSiH₂SiH₂Cl, Cl₂SiHSiH₂Cl, and Cl₂SiHSiHCl₂),¹⁶ respectively.

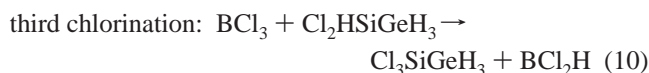
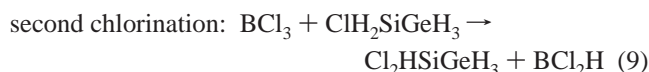
Simulation Studies of Cl_nH_{6-n}SiGe Molecules

(a) Reaction Thermochemistry. To complement the experimental studies and elucidate the origin of the chlorination reaction trends described above, we carried out a comprehensive simulation study of the Cl_nH_{6-n}SiGe molecules. Thermochemistry analysis of the chlorination reactions was carried out using the Gaussian03 program¹⁷ with a density functional theory description of the electronic structure at the B3LYP/6-311N++G-(3df,3pd) level. We have successfully used this approach in prior work to accurately describe the bonding, structure, and vibrational properties in related Si-Ge molecular hydride systems.^{6,8}

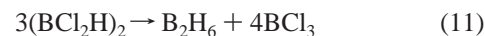
Here we use this approach to study the idealized general reactions involving the BCl₃ and H₃SiGeH₃, which can be written as depicted by eq 7.



This simple reaction model subsumes a number of side reactions involving intermediate species such as BCl₂H, BClH₂, SiCl₂H₂, GeH₄, and GeH₂. Of specific interest in this study are the chlorination reactions on the Si center of H₃SiGeH₃ described by eqs 8–10.



In all three of these reactions, the unstable BCl₂H product is initially produced and assumed to rapidly convert to diborane and BCl₃ via the well-known disproportionation reaction¹⁵ (eq 11)



which we do not consider here further. As a first step toward computing both the transition states involved in reactions 8–10, and standard reaction free energies based on eq 7, we calculated the equilibrium thermochemistry of all reactants and products. The ground state structures, the zero-point energy (ZPE) corrected electronic energies (*E*₀ + ZPE), and thermally corrected Gibbs free energies at 298 K (*G*_{TH}), of all pertinent reactants and products, are provided in Figures 2 and 3. All structural optimizations were performed using “tight” force convergence criteria. Figure 2 lists the structures and energies of reactants and products (other than the title Cl_nH_{6-n}SiGe compounds) such as BCl₃, B₂H₆, BHCl₂, and H₃SiGeH₃ produced in the reactions shown by eqs 7–10. The corresponding data for the title compounds Cl_nH_{6-n}SiGe (*n* = 1, ..., 4) is provided in Figure 3. Note that this list does not include all possible “trans” and “gauche” isomeric forms displayed by the heterochlorinated ClH₂SiGeH₂Cl, Cl₂HSiGeH₂Cl, ClH₂SiGeHCl₂, and Cl₂HSiGeHCl₂ derivatives. We find that the energy difference between isomers of the same compound is typically 10 kJ/mol but that their vibrational spectra are distinct. In this study, we consider the lowest energy isomer in each case as shown in Figure 3. The molecules are ordered according to the number of Si-Cl bonds (followed by the number of Ge-Cl bonds). A complete account of the role of isomers in the interpretation of the thermochemistry and vibrational spectra of chlorinated silylgermanes will be presented in a forthcoming publication.

(16) Sollradl, H.; Hengge, E. *J. Organomet. Chem.* **1983**, *243*, 257–269.

(17) Frisch, M. J. et al. *Gaussian 03*, Revision B.04; Gaussian Inc.: Wallingford, CT, 2004.

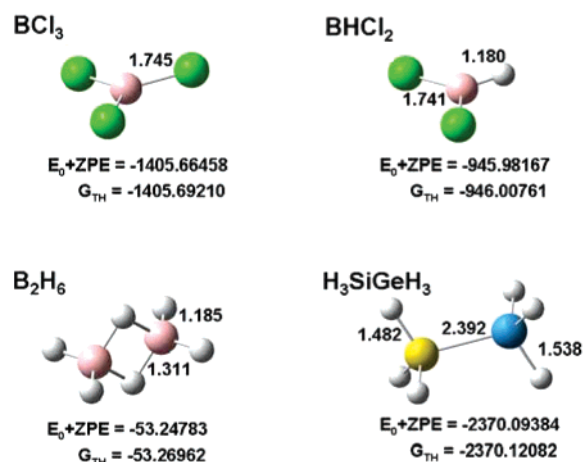


Figure 2. Equilibrium structures of BCl_3 , BHCl_2 , B_2H_6 , and H_3SiGeH_3 . Listed within the figure are the bond lengths (\AA), zero-point energy (ZPE) corrected electronic energies, and thermally corrected Gibbs free energies at 298 K (energies in Hartree). Legend: Si, yellow; Ge, blue; Cl, green; B, pink; H, white.

A primary goal of this study is to elucidate, on energetic and structural grounds, the chlorination trends in our compounds shown in Table 1. We note that the list of compounds presented in Figure 3 is augmented to include the $\text{Cl}_3\text{SiGeH}_3$ species (which was expected but not observed) as well as the compounds $\text{H}_3\text{SiGeH}_2\text{Cl}$, $\text{H}_3\text{SiGeHCl}_2$ with Cl atoms bound exclusively to Ge. The latter have been tentatively observed but not on a reproducible basis. This is presumably due to their relative instability with respect to decomposition or additional chlorinations at their Si sites to produce molecules containing at most four chlorine atoms combined, as observed.

Collectively, the structures shown in Figure 3 reveal the following general bonding trends: The Si–Ge bond has a typical value $\sim 2.40 \text{ \AA}$, which increases slightly in response to the repulsion due to the number of chlorine atoms on Si and Ge sites. The attachment of chlorine to Si and Ge also induces systematic variations in the Si–H and Ge–H bonds, which are found to lie in the ranges $1.471\text{--}1.482$ and $1.533\text{--}1.580 \text{ \AA}$, respectively. Variations of comparable magnitude are found in the Si–Cl and Ge–Cl bond lengths which exhibit values $2.053\text{--}2.077$ and $2.171\text{--}2.193 \text{ \AA}$, respectively.

We calculated standard reaction free energies, ΔG_{RX} at 298 K, following the generalized reaction given in eq 7, using the thermally corrected free energies listed in Figures 2 and 3. Our main results are provided in Table 3, which lists the reaction free energies in order of decreasing magnitude. As can be seen from this data, the relative stability of the chlorinated products is directly related to the number of Si–Cl bonds, and not the total number of bound chlorine atoms. This is consistent with the experimentally observed order of chlorination in which the first and second chlorination reactions occur exclusively on the Si center, followed by progressive chlorination of the Ge site. Note that the experimentally elusive $\text{H}_3\text{SiGeH}_2\text{Cl}$ and $\text{H}_3\text{SiGeHCl}_2$ compounds are the least stable due to the absence of Si–Cl bonds. In contrast, the most thermodynamically stable derivative $\text{Cl}_3\text{SiGeH}_3$ was never obtained despite systematic efforts to promote its formation. As we discuss below in detail, this is likely due to slow reaction kinetics.

The key role of Si–Cl bonding in the chlorination thermochemistry can be readily understood in terms of bond enthalpies,

ΔH , which provide a useful, but less rigorous, guide to understanding the salient bonding trends. To obtain these bond energies, we utilized atomization values which we calculated from the most basic gaseous species such as H_2 , B_2H_6 , BCl_3 , SiH_4 , GeH_4 , SiCl_4 , GeCl_4 , and H_3SiGeH_3 at the B3LYP/6-311G++(2d,2p) level of theory. Using this approach, we obtained the following: $\Delta H[\text{H–H}] = 110 \text{ kcal/mol}$, $\Delta H[\text{B–Cl}] = 104 \text{ kcal/mol}$, $\Delta H[\text{B–H}] = 76 \text{ kcal/mol}$, $\Delta H[\text{Si–H}] = 87 \text{ kcal/mol}$, $\Delta H[\text{Ge–H}] = 73 \text{ kcal/mol}$, $\Delta H[\text{Si–Cl}] = 96 \text{ kcal/mol}$, $\Delta H[\text{Ge–Cl}] = 77 \text{ kcal/mol}$, and $\Delta H[\text{Si–Ge}] = 47 \text{ kcal/mol}$. Using these values, the gas-phase chlorination reaction enthalpies ΔH_{BX} based on eq 7 were calculated and are given in Table 3. Note that these follow closely the trends obtained using the full thermochemistry analysis (see ΔG_{TH} in Table 3). In particular, the ordering predicated by the number of Si–Cl bonds formed is properly reproduced although the finer details are missed.

(b) Reaction Kinetics. The surprising absence of $\text{Cl}_3\text{SiGeH}_3$ in the reaction products in spite of its apparent thermodynamic stability prompted us to conduct a brief study of the transition state structures associated with first, second, and third Si site chlorination reactions given in eqs 8, 9, and 10, respectively. The transition states (TS) were initially optimized at the B3LYP/6-311G++(2d,2p) level using the Berny algorithm as implemented in the Gaussian03 program (n.b., all transition state thermochemistry calculations were carried out at 298 K). The reaction of BCl_3 and SiH_3GeH_3 (see eq 8) likely proceeds by electrophilic attack of a silyl proton by BCl_3 as shown in Figure 4 where the nucleophilic and electrophilic site reactivities of BCl_3 and H_3SiGeH_3 are compared on the basis of their self-consistent molecular electrostatic potentials (MEP), obtained at the B3LYP/6-311G++(3df,3pd) level. The latter are mapped onto appropriate isodensity surfaces and color coded according to local MEP value. Negative and positive regions are susceptible to electrophilic/nucleophilic attack, respectively. Accordingly, our calculations indicate that the electrophilic attack of silyl protons by BCl_3 , as indicated in Figure 4a, is the most likely reaction mechanism, due to the large MEP difference associated with the reaction sites indicated. On the basis of a plausible suggestion by Van Dyke and MacDiarmid we explored numerous possibilities for the structure of the first chlorination transition state complex¹⁵ involving four centered Si–H–B–Cl configurations as shown in Figure 5. Our initial search using the smaller but more efficient basis set yielded a TS configuration with two soft modes: one associated with a four-member transition state involving the transfer of Cl to Si and H to B, and the other involving the internal rotation of the terminal germlyl group. Subsequent TS optimization using the full B3LYP/6-311N++G(3df,3pd) prescription then produced a final transition state configuration possessing only a single soft mode ($i297 \text{ cm}^{-1}$). This indicates that the previously used small set did not have the accuracy to provide the uniquely resolved single soft mode. The latter represents the motion of the system across the barrier leading to the chlorine–hydrogen exchange on the Si site. The optimized structure of $\text{ClH}_2\text{SiGeH}_3$ (**1**) was then used as a starting point for the second chlorination reaction (eq 9) and the second chlorination product, $\text{Cl}_2\text{HSiGeH}_3$ (**2**), was then in turn used to initialize the third chlorination simulation. Using this approach, all three transition states were located, and the results are summarized in Figure 5. The

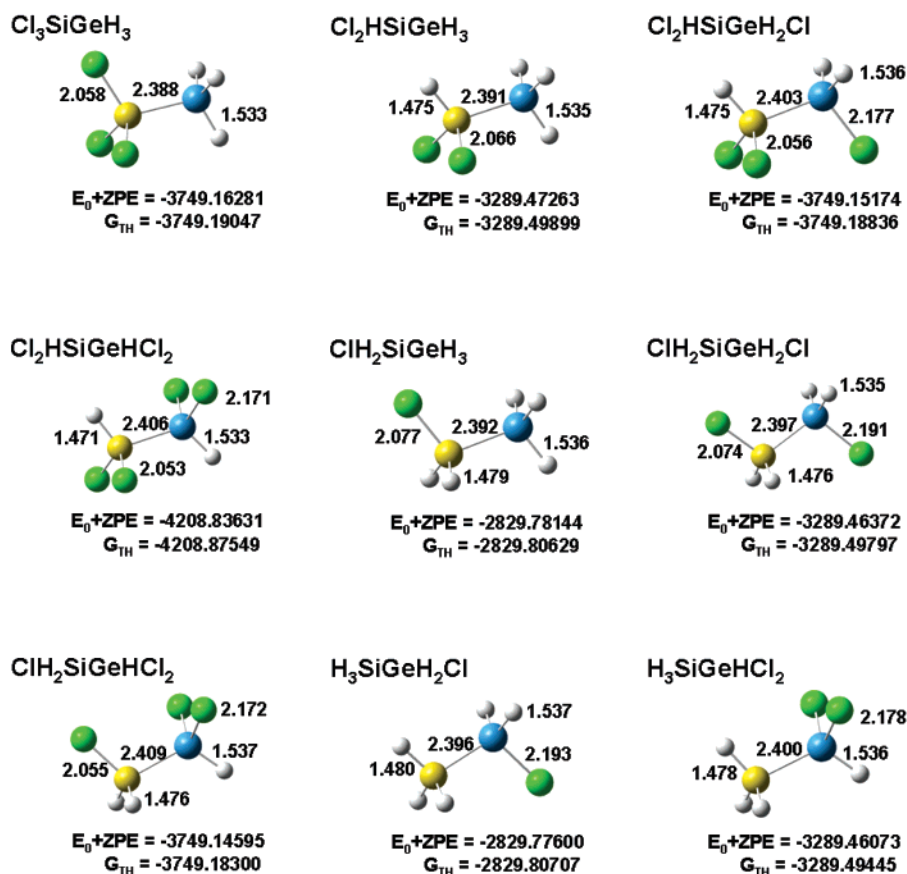


Figure 3. Equilibrium structures for the 9 Cl_nH_{6-n}SiGe molecules described in this study. Bond lengths are listed in Å, while the zero-point energy (ZPE) corrected electronic energies and thermally corrected Gibbs free energies at 298 K are given in Hartrees. Legend: Si, yellow; Ge, blue; Cl, green; H, white.

Table 3. Standard Reaction Free Energies ΔG_{RX}^a for Chlorination Reaction Products and Reaction Enthalpies ΔH_{RX} Obtained from Bond Enthalpy Calculations

ΔG _{RX} (kJ/mol)	ΔH _{RX} (kJ/mol)	product
-50.6	-79	Cl ₃ -Si-Ge-H ₃
-34.1	-53	Cl ₂ H-Si-Ge-H ₃
-26.9	-59	Cl ₂ H-Si-Ge-H ₂ Cl
-30.5	-81	Cl ₂ H-Si-Ge-HCl ₂
-14.9	-27	ClH ₂ -Si-Ge-H ₃
-14.7	-32	ClH ₂ -Si-Ge-H ₂ Cl
-12.8	-38	ClH ₂ -Si-Ge-HCl ₂
-1.3	-6	H ₃ -Si-Ge-H ₂ Cl
-5.5	-11	H ₃ -Si-Ge-HCl ₂
0.0	0	H ₃ -Si-Ge-H ₃

^a Thermally corrected values at 298 K.

magnitude of the forward reaction barrier (indicated as a 298 K Gibbs free energy difference in the figure) increases systematically through the chlorination sequence (33, 38, and 41 kcal/mol, respectively), while the free energy difference between products and reactants decreases. The interatomic distances of the “four center” configuration in the activated complex, and the corresponding soft mode frequencies (ω_{TS1} , ω_{TS2} , ω_{TS3}) associated with the transition states, are given in Figure 5b. The displacement patterns associated with the barrier crossing for the first and second chlorination soft modes involve primarily a motion of the “four-center” constituents while the rest of the complex remains essentially motion free. The normal mode associated with the third chlorination reaction, however, involves a similar motion of the entire four member complex, but also includes an additional collective “rocking” type

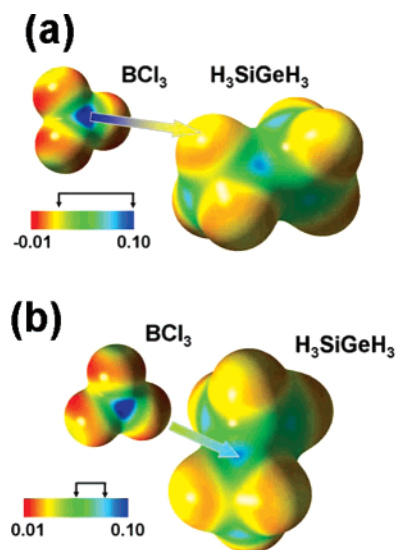


Figure 4. Molecular electrostatic potential (MEP) interpretation of site reactivity in the BCl₃-H₃SiGeH₃ reaction: (a) The arrow connects the reactive sites involved in the electrophilic attack of a silyl proton by BCl₃. (b) Nucleophilic attack of the Si site by the Cl. The arrow indicates a possible attack site along the Si-Ge backbone, near the Si atom (in this frame the H₃SiGeH₃ is oriented with the Si downward). The color bars indicate the common range of the MEP (in atomic units) which has been mapped onto isodensity contours of the BCl₃ and H₃SiGeH₃ molecules. Note that the MEP differences corresponding to the reaction sites shown (indicated by arrowed brackets above the MEP scale bars) are larger for the electrophilic process.

movement of the two heavy constituent Cl atoms bonded to Si. The latter may contribute to the slower kinetics associated with

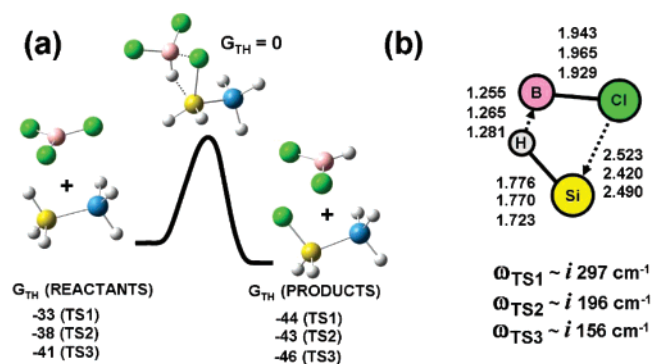


Figure 5. Transition state data for the three chlorination reactions of the Si site. (a) Structures of the reactant molecules, transition state complex, and product molecules. Dashed lines in the TS configuration indicate the bonds being “broken”. The thermally corrected Gibbs free energies (298 K) of the reactant and product states are given in kcal/mol relative to the transition state, which is taken as the reference value ($G_{\text{TH}} = 0$). The first, second, and third chlorination values are listed top to bottom, respectively. (b) Four center TS configuration involving transfer of the Si–H proton to the BCl_3 molecule, and binding of chlorine to the Si site. Bond lengths for the individual first, second, and third chlorination reactions are listed top to bottom, respectively. The corresponding soft mode frequencies for the transitions state complexes are listed as ω_{TS1} , ω_{TS2} , and ω_{TS3} .

the third chlorination of the molecule. Furthermore, for the third chlorination the thermodynamic driving force associated with ΔG_{TH} (where $\Delta G_{\text{TH}} = G_{\text{TH products}} - G_{\text{TH reactants}}$) is the smallest (5 kcal/mol), and the reaction barrier is the largest (41 kcal/mol), while the first chlorination step involves a net reaction energy gain of 11 kcal/mol and a barrier of 33 kcal/mol. In combination, these observations suggest that the third chlorination is clearly less favorable than the first or second. Accordingly, the $\text{Cl}_3\text{SiGeH}_3$ compound was never observed under our reaction conditions. Careful analysis of the reaction products did not reveal the presence of trichlorosilane (SiHCl_3) which is expected to be the most stable decomposition byproduct of $\text{Cl}_3\text{-SiGeH}_3$, ruling out the transient formation of this compound followed by its decomposition.

(c) Vibrational Properties of $\text{ClSiH}_2\text{GeH}_3$ and $\text{Cl}_2\text{SiHGeH}_3$. The vibrational properties of all compounds described in Figures 2 and 3 were obtained as a byproduct of the thermochemical analyses discussed above. Here we specifically describe the IR spectra of only compounds $\text{ClSiH}_2\text{GeH}_3$ (**1**) and $\text{Cl}_2\text{SiHGeH}_3$ (**2**), which were fully isolated as pure volatile products and utilized in proof of concept CVD applications. The vibrational spectra of the remaining compounds will be reported elsewhere. In previous investigations, we successfully used simulated vibrational spectra to identify the various positional and conformational isomers in a mixture of butane-like $\text{GeH}_3\text{SiH}_2\text{SiH}_2\text{GeH}_3$ and $\text{GeH}_3\text{GeH}_2\text{SiH}_2\text{GeH}_3$ compounds.⁸ Here we use this approach to corroborate the molecular structures (Figure 3) of the purified **1** and **2** as derived from the NMR spectra.

The spectra of both **1** and **2** molecules were obtained using the full B3LYP/6-311N++G(3df,3pd) prescription. The normal modes exhibited positive definite vibrational frequencies, indicating that the ground state structures are dynamically stable. Symmetry analysis of the optimized structures indicates that the molecules are asymmetric tops possessing C_s symmetry. In general, the high-frequency spectra of both compounds contain two primary features corresponding to asymmetric and symmetric Ge–H stretches ($2120\text{--}2160 \text{ cm}^{-1}$) and their asymmetric

Table 4. Unscaled Harmonic Vibrational Frequencies of $\text{ClH}_2\text{SiGeH}_3$ (**1**) and $\text{Cl}_2\text{HSiGeH}_3$ (**2**) Given in Parentheses (cm^{-1}) and Corresponding Assignments^a

	$\text{ClSiH}_2\text{GeH}_3$		$\text{Cl}_2\text{SiHGeH}_3$
“Sil” (119)	SiCl rocking	C_{v1} (125)	s SiCl ₂ rocking
		C_{v2} (189)	Si–Cl scissor
B_{v1} (333)	Si–Ge stretch	C_{v3} (320)	Si–Ge stretch
B_{v2} (361)	s SiH ₂ /GeH ₂ wagging	C_{v4} (448)	s GeH ₂ wagging
B_{v3} (471)	a GeH ₃ + SiH ₂ rocking	C_{v5} (467)	a GeH ₃ rocking
B_{v4} (530)	Si–Cl stretch	C_{v6} (520)	s Si–Cl stretch
B_{v5} (702)	a SiH ₃ rocking	C_{v7} (559)	a Si–Cl stretch
B_{v6} (780)	s GeH ₃ /SiH ₂ rocking	C_{v8} (746)	s GeH ₃ /SiH rocking
B_{v7} (840)	a GeH ₃ /SiH ₂ rocking	C_{v9} (787)	SiH wagging
B_{v8} (890)	a GeH ₃ wagging	C_{v10} (808)	a GeH ₃ /SiH ₂ rocking
B_{v9} (950)	s SiH ₂ wagging	C_{v11} (873)	a GeH ₃ wagging
b_{v1} (2142)	s GeH ₃ stretch	c_{v1} (2113)	s GeH ₃ stretch
b_{v2} (2146)	a GeH ₃ stretch	c_{v2} (2124)	a GeH ₂ stretch
b_{v3} (2224)	s SiH stretch	c_{v3} (2132)	a GeH stretch
b_{v4} (2236)	a SiH stretch	c_{v4} (2241)	SiH stretch

^a Given as s = symmetrical, a = asymmetrical, or “sil” for silent modes with zero calculated intensity.

and symmetric Si–H counterparts ($2220\text{--}2240 \text{ cm}^{-1}$). The corresponding low-frequency spectra ($200\text{--}1200 \text{ cm}^{-1}$) are significantly more complex, and normal mode assignments are given in Table 4. General assignments for both molecules, by frequency range, are as follows: (i) $120\text{--}160 \text{ cm}^{-1}$, Si–Cl rocking modes; (ii) $320\text{--}350 \text{ cm}^{-1}$, Si–Ge stretching; (iii) $520\text{--}530 \text{ cm}^{-1}$, Si–Cl stretches; (iv) $380\text{--}480 \text{ cm}^{-1}$, asymmetric $\text{GeH}_3/\text{SiH}_x$ rocking vibrations; (v) $740\text{--}800 \text{ cm}^{-1}$, symmetric $\text{GeH}_3/\text{SiH}_x$ rocking vibrations; and (vi) $800\text{--}950 \text{ cm}^{-1}$, various GeH_3 and SiH_x wagging vibrations. Among these assignments, the group v $\text{GeH}_3/\text{SiH}_x$ rocking modes are the most intense. These have almost the same frequency in both molecules and are designated as B_{v6} (780 cm^{-1}) and C_{v8} (787 cm^{-1}) in $\text{ClSiH}_2\text{-GeH}_3$ (**1**) and $\text{Cl}_2\text{SiHGeH}_3$ (**2**) molecules, respectively, as shown in Table 4.

A detailed comparison of the calculated and observed spectra of compounds **1** and **2** is presented in Figure 6. On the basis of our prior simulation work using comparable basis sets and model chemistries, we have applied the 0.989 and 0.979 frequency scale factors to the calculated the low- and high-frequency spectra, respectively.^{6,8} As can be seen from the figure, the calculated frequencies and intensities of both compounds match their experimental counterparts very closely, suggesting that the mode assignments listed in Table 4 are reliable. We note that while a common scale factor is used here for both compounds, a slight adjustment of the high-frequency factor (0.979) used in Figure 5b could improve the individual agreement for each compound further. We note that the simple harmonic vibrational analysis presented here does not account for the significant splittings ($10\text{--}15 \text{ cm}^{-1}$) observed for the vibrational bands in the experimental spectra of both $\text{ClH}_2\text{SiGeH}_3$ and $\text{Cl}_2\text{HSiGeH}_3$. We have investigated several possible origins for this splitting, including dimeric interactions and roto–vib couplings. Test calculations on $(\text{ClH}_2\text{SiGeH}_3)_2$ dimers indicate that only a select number of vibrational features are split, depending upon their relative configurations, when molecules are dimerized. Therefore, since dimerization does not split all peaks equally, we dismiss this mechanism. In addition, the dimeric interaction strengths are estimated to be only a few tenths of a kcal/mol, and dimerization is therefore not likely to occur at room temperature. We next examined the effects of roto–vib coupling

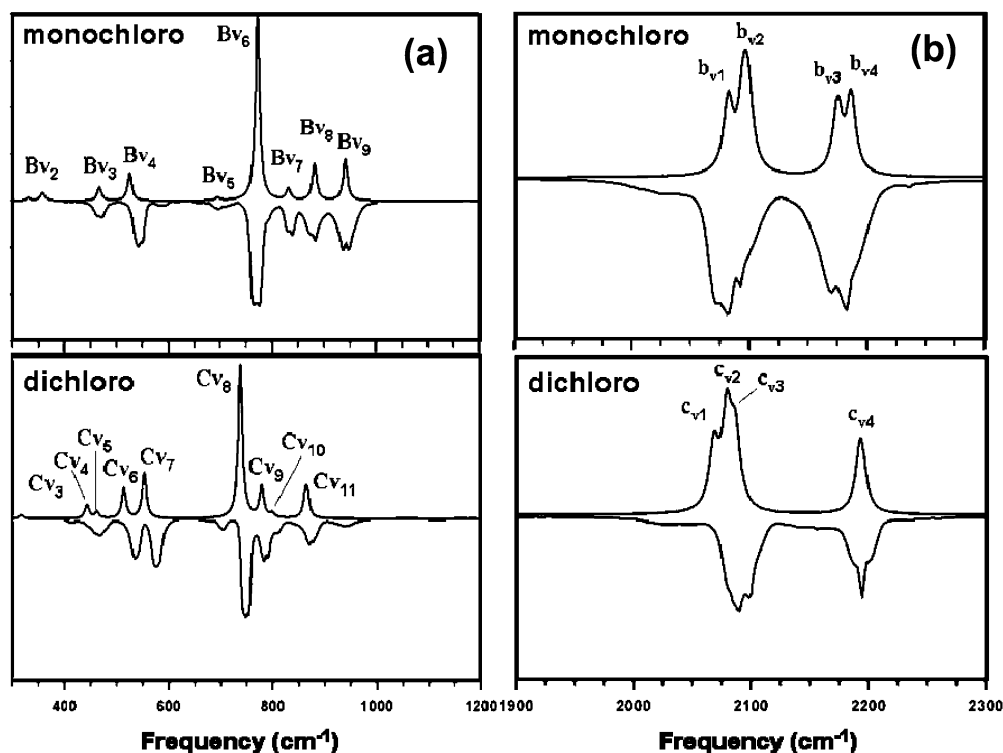


Figure 6. Comparisons of the calculated and observed room-temperature IR spectra of molecules **1** and **2**. Frequency scale factors of 0.989 and 0.979 were applied to the calculated low- and high-frequency spectra, shown in parts a and b, respectively.

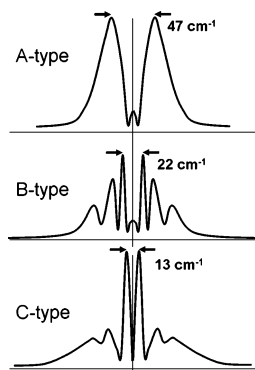


Figure 7. Simulated rotational band contours of A-, B-, and C-type bands obtained using calculated rotational constants for ClH₂SiGeH₃.

at room temperature in these asymmetrical top molecules. Our analysis revealed that roto-vib coupling produces splittings in all bands, including the high-frequency Ge–H and Si–H modes in both molecules. This can be explained by the relatively low symmetry of the ClH₂SiGeH₃ and Cl₂HSiGeH₃ molecules, which leads to A-type symmetries for all vibrational modes (e.g., no A' or A'' symmetry vibrations). As an example, using our calculated rotational constants for the ClH₂SiGeH₃ molecule ($A = 10.18$ GHz, $B = 1.42$ GHz, $C = 1.29$ GHz), we have computed the room-temperature rotational band profiles corresponding to A-, B-, and C-type contours using an asymmetrical top computer program. These are compared in Figure 7 which indicates that the possible profiles are quite distinct and that the C-type contour closely matches to the observed absorption band shapes with an apparent splitting of approximately ~ 13 cm⁻¹. The dichloro rotational constants give rise to very similar splittings which further corroborate the origin of these spectral features.

Pseudomorphic Growth of Si_{1-x}Ge_x

Proof-of-principle growth experiments were conducted to investigate the applicability of compounds ClH₂SiGeH₃ (**1**) and Cl₂HSiGeH₃ (**2**) to form semiconductor alloys at low temperatures. The growth studies were conducted on Si(100) substrates in an ultrahigh vacuum (UHV) deposition system. The substrates were prepared for growth by flashing at 1000 °C under UHV (10^{-10} Torr) to remove the native oxide from the surface. The gaseous precursors **1** or **2** were then reacted on the clean Si surface to form films via desorption of HCl and H₂ byproducts.

(a) ClH₂SiGeH₃ Growth Studies. The depositions of ClH₂SiGeH₃ were conducted at partial pressure and reaction temperatures typically in the range of 10^{-5} – 10^{-6} Torr and 360–450 °C, respectively. The film composition was determined by Rutherford backscattering (RBS) to be Si_{0.50}Ge_{0.50} reflecting precisely the Si/Ge ratio of the ClH₂SiGeH₃ precursor. The heteroepitaxial character of the synthesized films was initially investigated by random and channeling RBS, which indicates that the material is perfectly aligned with the substrate. The ratio of the aligned versus the random peak heights (χ_{\min}), which measures the degree of crystallinity, decreases from 25% at the interface to 10% at the surface indicating a typical defect “pile up” near the interface while the upper portion of the film is relatively defect-free. The film crystallinity was thoroughly investigated by high-resolution cross sectional electron microscopy (XTEM) which revealed commensurate SiGe/Si interfaces and perfectly monocrystalline epilayer microstructure. The TEM samples showed very few defects penetrating through the layers, which is consistent with the RBS dechanneling due to defect pile-up near the interface. High-resolution X-ray diffraction (HR-XRD) revealed perfectly aligned layers with low mosaic spread and slightly strained microstructures as grown. A nominal XRD relaxation of 75% was observed for a film thickness ~ 80 nm.

Atomic force microscopy (AFM) scans over areas $10 \times 10 \mu\text{m}^2$ show that films with thickness of 80 and 100 nm display rms values of 0.7 and 1.1 nm, respectively, indicating highly planar surfaces. We note that no “cross hatched” surface patterns, caused by misfit dislocations produced during strain relaxation, were observed even for films annealed up to 700 °C. In fact, the surface roughness either remained the same or improved slightly with annealing indicating that the planarity of our samples is thermally robust.

(b) $\text{Cl}_2\text{HSiGeH}_3$ Growth Studies. The deposition of $\text{Cl}_2\text{HSiGeH}_3$ (**2**) was conducted at 450 °C (10^{-5} Torr) and produced films with thickness ranging from 10 to 80 nm at growth rates approaching 1 nm/min, which is slightly higher than that obtained from the deposition of **1**. For films exceeding 10–20 nm in thickness, a quantitative analysis based on RBS showed that the Si content can be as low as 43%. For thinner samples (<10 nm), the film composition was derived from high-resolution XRD data because the Si content was difficult to extract from the substrate background using RBS. For thicker samples, we observed a systematic reduction from the expected (ideal) 50% stoichiometry when the deposition pressure is reduced from 5×10^5 to 1×10^5 Torr. Silicon depletion is likely enhanced under the lower pressure conditions due to facile surface desorption of multichlorinated Si species, such as stable SiH_2Cl_2 decomposition byproducts. The crystallographic alignment and surface morphology of these films were found to be of comparable quality to those obtained from depositions of **1**. Nevertheless, their XTEM characterizations showed lower threading dislocation densities of the layers, and superior microstructural quality of the interface regions. This includes flawless epitaxial registry and atomically abrupt transitions between the film and the substrate, consistent with the absence of elemental intermixing between the two materials at the low growth temperatures.

The strain state properties of the films were extensively characterized using HR-XRD. Here we focus on two representative samples with layer thicknesses of ~ 10 and 60 nm. Precise in-plane and perpendicular lattice constants were determined by high resolution (224) and (004) on- and off-axis reciprocal space maps of the entire structure. In the case of the thinner sample, the XRD data revealed that the growth produces two discernible layers in which the initial layer adjacent to the interface is fully strained to the Si substrate ($a_{\parallel} = a_{\text{Si}} = 5.4309 \text{ \AA}$ and $a_{\perp} = 5.5991 \text{ \AA}$) and has a thickness of 5–7 nm (see Figure 8). With elementary elastic strain relations¹⁸ ($\epsilon_{\perp} = -2C_{12}/C_{11}\epsilon_{\parallel}$ where C_{11} and C_{12} are bulk SiGe elastic constants, and ϵ_{\perp} and ϵ_{\parallel} are the perpendicular and parallel strains), the known bowing behavior of bulk Si–Ge alloys, and the structural data above, the composition of the initial alloy layer was determined to be $45 \pm 2\%$ Ge and $55 \pm 2\%$ Si. The XRD data also showed a diffuse, high mosaicity peak (peak 1 in Figure 8) indicating that the upper portion of the film (grown following the initial layer) is 50% relaxed and has lattice constants $a_{\parallel} = 5.4845 \text{ \AA}$ and $a_{\perp} = 5.5654 \text{ \AA}$ corresponding to a composition of $\sim 47 \pm 2\%$ Ge and $53 \pm 2\%$ Si. This indicates that this upper layer possesses stoichiometries closer to the expected 50/50 value in accordance with precursor Si–Ge content. In this diffusion-limited low-temperature growth process, the tendency to strain-match with Si can only be achieved by incorporation of excess

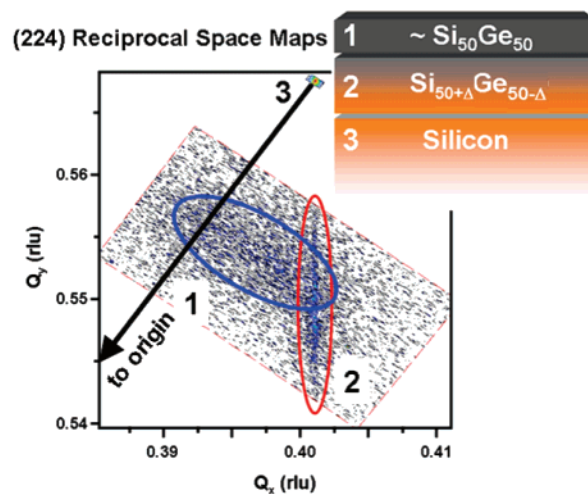


Figure 8. (224) reciprocal space maps of the 10 nm thick sample and the Si substrate, showing peaks 1 and 2 for the two layer structure. Note that 2 (corresponding to the layer adjacent to the interface as shown in the schematic inset) falls directly below the Si (224) peak indicating perfect lattice matching within the interface plane. Its elongation is due to the small thickness of the layer. A more diffuse peak 1 is also clearly visible and corresponds to the upper portion of the film. Note that peak 1 lies below the relaxation line connecting the Si peak to the origin, indicating partial relaxation ($\sim 50\%$).

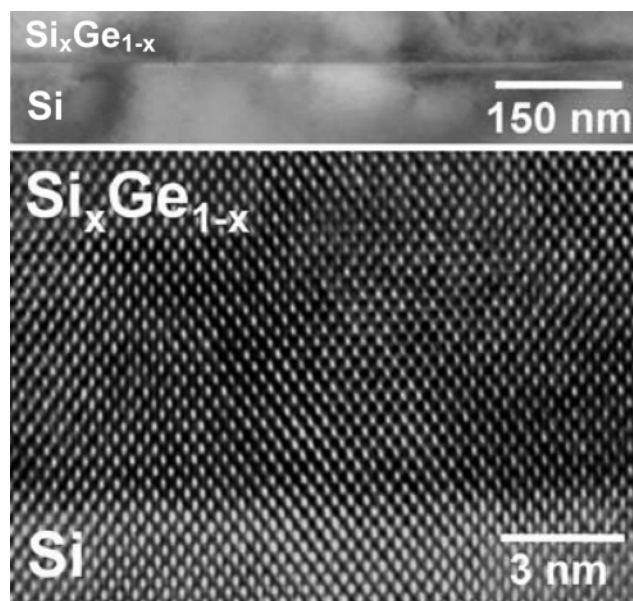


Figure 9. (Top) XTEM micrograph of the entire film thickness showing flat surface and bulk region devoid of defects. (Bottom) High-resolution micrograph of the interface region showing perfect pseudomorphic growth.

Si at the interface layer. Beyond a certain critical thickness (~ 50 – 60 \AA under these conditions), the strain is gradually relieved without any measurable defect formation, enabling the full stoichiometry of the precursors to be incorporated.

In the case of the 60 nm thick film, we observe that the growth also produces the same initial fully strained layer (~ 10 nm thick) adjacent to the interface, followed by a transition to a partially strained bulk film whose Si content approaches nominal target values. Figure 9 shows an XTEM micrograph of the entire film thickness in (100) projection. Note that the film surface is atomically flat and the bulk material is devoid of threading defects within a wide field of view (typically $2 \mu\text{m}$). The high-resolution image of the interface region shows

(18) Brantley, W. A. *J. Appl. Phys.* **1973**, *44*, 534.

perfect commensuration and no indication of misfit dislocations in spite of the large mismatch. This observation is consistent with full pseudomorphic growth as determined by XRD. The lack of defects can be explained by our observation of an inherent compositional gradient which accommodates the strain throughout the film. These mechanisms are unique to the low-temperature growth protocol afforded by the specifically designed precursor chemistry employed in this study.

Concluding Remarks

The synthesis of Cl_nH_{6-n}SiGeH₃ is achieved via selective chlorination of SiH₃GeH₃ by BCl₃ at low temperatures. The ClH₂SiGeH₃ species is also formed via reaction of (SO₃-CF₃)SiH₂GeH₃ and CsCl using a complex multistep reaction route based on PhSiH₂GeH₃ low yield intermediates. Detailed characterization of the products was conducted via a range of spectroscopic and analytical methods including quantum chemical simulations of the reaction thermodynamics and kinetics. Low-temperature depositions of ClH₂SiGeH₃ (**1**) and Cl₂-HSiGeH₃ (**2**) have produced near stoichiometric Si_xGe_{1-x} films ($x = 0.43-0.55$ depending on deposition conditions) possessing the desired properties for semiconductor applications including perfectly crystalline and epitaxial microstructures, smooth morphologies, and unique strain/relaxed states.

We have previously utilized SiH₃GeH₃ and the butane-like (GeH₃)₂(SiH₂)₂ compound to deposit Si_{0.50}Ge_{0.50} films at low temperatures. In both cases, we have obtained materials with high quality morphological and microstructural properties. Nevertheless, the use of SiH₃GeH₃ for low-temperature CMOS selective growth of small size device features is not practical due to the dramatic drop in growth rates below 475 °C (negligible below 450 °C). In contrast, both ClH₂SiGeH₃ and (GeH₃)₂(SiH₂)₂ yield growth rates at least 10 times higher than those obtained from SiH₃GeH₃ in the 400–450 °C range, and these compounds even display significant film growth at temperatures below 400 °C. It should also be noted that the film quality is comparable using either ClH₂SiGeH₃ or (GeH₃)₂(SiH₂)₂ to grow Si_{0.50}Ge_{0.50}. However, albeit (GeH₃)₂(SiH₂)₂ shows promise from a technical perspective, it represents a demonstration in principle rather than a true proof of concept from an industrial perspective. For instance, this compound is difficult to synthesize in quantities greater than a few grams, and its thermal stability in relation to storage and transportation is not well understood. Thus, the ClH₂SiGeH₃ (**1**) and Cl₂H₂-SiGeH₃ (**2**) counterparts appear to be more practical candidates for immediate deployment as a 50/50 SiGe source. Their synthesis is much easier to scale up, and the starting materials are readily available and inexpensive. The single step reaction of BCl₃ with H₃SiGeH₃ is conducted in a solvent free environment ensuring facile isolation and purification to produce semiconductor grade material. Further, due to their high vapor pressure, the compounds can be readily integrated with existing commercial processes involving single-wafer low-pressure CVD furnaces. Future work in this area will be focused on the use of these compounds in selective deposition applications using patterned substrates provided by ASM international.

Experimental Section

General Methods. All manipulations were carried out under inert conditions using standard high vacuum line and drybox techniques. Dry, air-free solvents were distilled from either anhydrous CaCl₂ or

sodium benzophenone ketyl prior to use. The NMR spectra were collected on an Inova 500 MHz spectrometer. Samples were dissolved in deuterated benzene, and all nuclei were referenced either directly or indirectly to the signal of TMS or the residual solvent peak as indicated. Gaseous infrared spectra were obtained in 10-cm cells fitted with KBr windows. Mass spectrometry data were obtained using a Leybold-Inficon quadrupole mass spectrometer. Boron trichloride (Aldrich 99.95%) was distilled to remove residual HCl contaminants, and its purity was confirmed by infrared and mass spectra prior to use. Lithium tetrahydroaluminate (Aldrich), phenyl trichlorosilane (Aldrich), trifluoromethane sulfonic acid (Alfa Aesar), cesium chloride (Aldrich), and electronic grade germane gas (donated by Voltaix, Inc.) were used as received. The starting materials include phenylsilane, which was prepared by reduction of phenyl trichlorosilane with LiAlH₄, and phenyl monochlorosilane, which was prepared by the reaction of phenylsilane with gaseous HCl. Phenylsilylgermane,¹⁴ germysilyl trifluoromethanesulfonate,⁶ and germysilane⁶ were prepared according to literature procedures. All starting materials were checked by NMR spectroscopy to verify their purities. Potassium germyl (KGeH₃) was synthesized via a modified literature preparation in monoglyme by reaction of gaseous GeH₄ with a finely dispersed sodium–potassium (80% K) alloy. Note that the Teflon bar that was used to stir the GeH₄/Na–K/monoglyme solution was encapsulated in glass owing to the high reactivity of Teflon with Na–K alloys.

Synthesis of Cl_nH_{6-n}SiGe: Method A. (a) Reaction of CsCl with (CF₃SO₃)SiH₂GeH₃. A 50 mL Schlenk flask was charged with n-decane (15 mL) and (CF₃SO₃)SiH₂GeH₃ (0.60 g, 2.35 mmol). Cesium chloride (0.42 g, 2.49 mmol) was added slowly via a powder addition funnel at –25 °C to the flask, and the mixture was allowed to stir under N₂ for 12 h at 22 °C. The volatiles were fractionally distilled through U-traps held at –50, –110, and –196 °C under dynamic vacuum. The –50 and –196 °C traps contained solvent and traces of GeH₄. The –110 °C trap retained pure, colorless **1** (0.186 g, 56% yield). Vapor pressure: ~147 Torr (23 °C). IR (gas, cm⁻¹): 2183 (vs), 2171 (s), 2156 (vw), 2092 (vw), 2082 (vs), 2070 (s), 1076 (vw), 948 (m), 936 (m), 896 (m), 839 (vw), 830 (vw), 790 (s), 774 (vs), 764 (vs), 549 (m), 540 (m), 470 (w), 360 (vw). ¹H NMR (500 MHz, C₆D₆): δ 4.68 (q, 2H, Si–H₂), δ 3.12 (t, 3H, Ge–H₃). ²⁸Si NMR (500 MHz, C₆D₆): δ –24.61. Mass spectrum: *m/z* isotopic envelopes centered at 141 (M⁺), 106 (H₃GeSiH₃⁺), 75 (GeH₄⁺), 65 ClSiH₂⁺, 36 (Cl⁺), 31 (SiH₄⁺). *Caution:* Mixtures of (SO₃CF₃)SiH₂GeH₃ have been found to explode.

Synthesis of Cl_nH_{6-n}SiGe: Method B. (a) Reaction of 1:3 BCl₃/H₃SiGeH₃. Gaseous BCl₃ (0.37 g, 3.2 mmol) and H₃SiGeH₃ (1.02 g, 9.6 mmol) were condensed into a 150 mL stainless steel cylinder at –196 °C equipped with a high vacuum valve. The cylinder and its contents were held at 0 °C for 2 h after which time the volatile contents were distilled through U-traps held at –78, –95, and –196 °C. The latter contained predominately B₂H₆ and unreacted H₃SiGeH₃ as evidenced by gas IR. The –95 °C trap contained pure **1** as evidenced by ¹H NMR. The liquid in the –78 °C trap was analyzed by ¹H NMR (500 MHz, C₆D₆) and was found to be a mixture of **1** and **2** [δ 5.57 (q, H, Si–H), δ 3.25 (d, 3H, Ge–H₃)]. The integrated ¹H peak intensities of the Ge–H₃ resonances indicated a ~12:1 ratio of **1** to **2**, which were separated by fractional distillation through –78 to –95 °C traps. This reaction yielded 5.70 mmol (~60% yield) of **1** and 0.48 mmol (5% yield) of **2**.

(b) Reaction of 2:3 BCl₃/H₃SiGeH₃. BCl₃ (0.33 g, 2.8 mmol) and H₃SiGeH₃ (0.45 g, 4.2 mmol) were condensed into a 150 mL stainless steel cylinder and allowed to react at 0 °C for 2 h after which time the volatiles were distilled through U-traps held at –78, –95, and –196 °C. The contents of the –78 °C traps were shown to be a mixture of **1** and **2** while those of the –95 °C trap were pure **1**. The yields for **1** and **2** were found to be 1.5 mmol (36%) and 1.3 mmol (31%), respectively. The –196 °C trap contained predominately B₂H₆ and unreacted H₃SiGeH₃.

(c) **Reaction of 1:1 BCl₃/H₃SiGeH₃**. BCl₃ (0.70 g, 6.0 mmol) and H₃SiGeH₃ (0.64 g, 6.0 mmol) were condensed into a 150 mL stainless steel cylinder and allowed to react for 2 h at 0 °C. The volatiles were then distilled through U-traps held at -35, -78, -110, and -196 °C. The -196 and -110 °C traps contained B₂H₆ (~3.0 mmol, 100% yield) and minor concentrations of Cl₂SiH₂. The -78 °C trap contained pure **2** as a clear, colorless liquid (1.5 mmol, 25% yield).

Cl₂SiHGeH₃ (2). Vapor pressure 40 Torr (23 °C), IR (gas, cm⁻¹) 2194 (s,sh), 2099 (w), 2091 (s), 876 (m), 869 (m), 792 (m), 783 (m), 753 (vs), 748 (vs), 706 (vw), 577 (s), 536 (m), 460 (w). Mass spectrum: *m/z* isotopic envelopes centered at 175 (M⁺), 141 (ClSiGeH₅⁺), 106 (H₃GeSiH₃⁺), 100 (Cl₂SiH₂⁺), 75 (GeH₄⁺), 65 (ClSiH₂⁺), 36 (Cl⁺), 31 (SiH₄⁺). ¹H NMR (500 MHz, C₆D₆): δ 5.57 (q, H, *J* = 3.0 Hz, Si-H), δ 3.25 (d, 3H, *J* = 3.0 Hz, Ge-H₃). ²⁹Si (500 MHz, C₆D₆): δ 9.77. 2D ¹H COSY confirmed that the ¹H resonances were coupled to each other. The ¹H-²⁹Si HMQC showed that the ¹H resonance at δ 5.57 (q) was directly coupled to the ²⁹Si resonance at δ 9.77.

Cl₂SiHGeH₂Cl (3), **Cl₂SiHGeHCl₂ (4)**, **ClSiH₂GeH₂Cl (5)**, and **ClSiH₂GeHCl₂ (6)**. The -45 °C trap contained a low volatility liquid (~2.0 Torr vapor pressure) which was characterized by NMR to be a mixture of polychlorinated silylgermanes. The ²⁹Si (500 MHz, C₆D₆) spectrum consisted of four peaks at δ -22.87, -24.26, -1.12, and 3.36, and the ¹H spectra (500 MHz, C₆D₆) showed eight peaks with chemical shifts at δ 6.12 (t), 5.97 (d), 5.35 (t), 5.15 (d), 4.86 (t), 4.82 (d), 4.53 (t), and 4.38 (d). These data collectively suggested the presence of four Cl_{*n*}H_{6-*n*}SiGe compounds. A ¹H-²⁹Si HMQC (500 MHz, C₆D₆) spectrum showed that the H atoms with resonances at δ 5.35, 5.15, 4.53, and 4.38 are bound to Si atoms with resonances at δ 3.36, -1.12, -24.26, and -22.87, respectively. ¹H 2D COSY experiments were performed to establish connectivities. Cross-peaks were found to be between the following pairs of [Si-H_{*x*}, GeH_{*x*}] resonances: [δ 4.38 (d), 6.12 (t)], [δ 5.15 (d), 5.97 (d)], [δ 4.53 (t), 4.86 (t)], and [δ 5.35 (t), 4.82 (d)]. The corresponding Si-H_{*x*}/GeH_{*x*} peak height ratios are 2:1, 1:1, 1:1, and 1:2, respectively. Accordingly, these can be assigned to the compounds ClSiH₂GeHCl₂ (**6**), Cl₂SiHGeHCl₂ (**4**), ClSiH₂GeH₂Cl (**5**), and Cl₂SiHGeH₂Cl (**3**), respectively.

Cl₂SiHGeH₂Cl. ¹H NMR: δ 4.82 (d, 2H, *J* = 4.3 Hz, Ge-H₂), δ 5.35 (t, H, *J* = 4.3 Hz, Si-H). ²⁹Si NMR: δ 3.36.

Cl₂GeHSiHCl₂. ¹H NMR: δ 5.15 (d, H, *J* = 7.0 Hz, Si-H), δ 5.97 (d, H, *J* = 7.0 Hz, Ge-H). ²⁹Si NMR: δ -1.12.

ClSiH₂GeHCl₂. ¹H NMR: δ 4.38 (d, 2H, *J* = 4.4 Hz, Si-H₂), δ 6.12 (t, H, *J* = 4.4 Hz, Ge-H). ²⁹Si NMR: δ -22.87.

ClSiH₂GeH₂Cl. ¹H NMR: δ 4.53 (t, 2H, Si-H₂), δ 4.86 (t, 2H, Ge-H₂). ²⁹Si NMR: δ -24.26.

(d) **Reaction of 2:1 BCl₃/H₃SiGeH₃**. Gaseous BCl₃ (0.55 g, 4.7 mmol) and H₃SiGeH₃ (0.25 g, 2.35 mmol) were reacted for 2 h at -196 °C in the stainless steel cylinder reactor. The volatile contents were then distilled through U-traps held at -35, -78, and -196 °C. The -196 °C trap contained B₂H₆, unreacted BCl₃, and a minor amount of SiH₂Cl₂. The -78 °C trap contained traces of Cl₂SiHGeH₃ (5% yield). The -35 °C trap contained the bulk product as a colorless low volatility liquid (~2.0 Torr vapor pressure) which consisted of ClSiH₂GeHCl₂, Cl₂SiHGeHCl₂, ClSiH₂GeH₂Cl, and Cl₂SiHGeH₂Cl as evidenced by extensive NMR studies (as described above for the 1:1 H₃SiGeH₃/BCl₃ reaction). The ¹H NMR resonance integration indicated that the predominant species were Cl₂SiHGeHCl₂ and Cl₂SiHGeH₂Cl, while ClSiH₂GeHCl₂ and ClSiH₂GeH₂Cl are present in very small amounts.

We finally note that most reactions described above using method B were conducted under 2 h intervals because longer times at the temperatures employed resulted in intractable polymers rather than molecular systems indicating that there are competing decomposition reactions under these conditions.

Acknowledgment. This research was supported by the U.S. Air Force Office of Scientific Research (AFOSR MURI, FA9550-06-01-0442), Voltaix Corporation, and NSF (IIP 053950). The XRD equipment used in this work was obtained by a grant from the NSF (DMR-0526604).

Supporting Information Available: Complete ref 17. This material is available free of charge via the Internet at <http://pubs.acs.org>.

JA0713680